Supplementary Materials

Simultaneous Magneto-dielectric Transition in a Fluorescent Hofmann-type Coordination Polymer

Fei-Fei Yan,[a] Dan Liu,[a] Rui Cai,[b] Liang Zhao,[a] Pan-Dong Mao,[a] Hui-Ying Sun,[a] Yin-Shan Meng,*[a] and Tao Liu*[a]

[a]*State Key Laboratory of Fine Chemicals, Dalian University of Technology, Dalian, 116024, China.*

[b]*Instrumental Analysis Center, Dalian University of Technology, Dalian, 116024, China.*

*Corresponding author. Email: mengys@dlut.edu.cn (Y.-S. Meng), liutao@dlut.edu.cn (T. Liu)

Contents

Experimental Section

Materials.

All chemical reagents were commercially available and used without further purification. The TPE-based ligand DPPE was prepared according to published literature.[1]

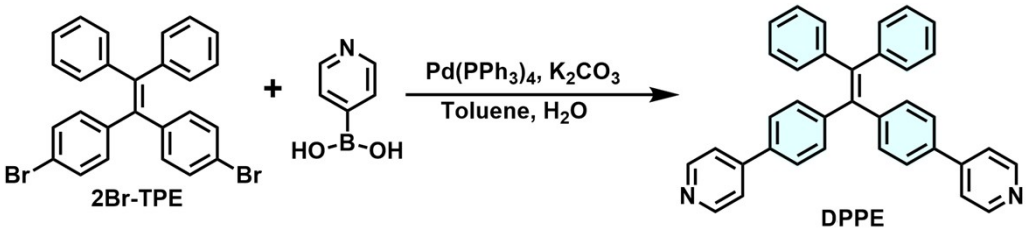

Scheme S1

Table S1. Selected bond lengths (Å) and bond angles (˚) for **1** at 120 K and 298 K.

Compound 1$^{120\ K}$			
Bond length (Å)			
Fe1–N1	2.022(4)	Fe1–N1^{2}	2.022(4)
Fe1–N2	1.977(7)	Fe1–N3	1.953(5)
Fe1–N3^{2}	1.953(5)	Fe1–N4^{3}	1.980(7)
Ag1–C1	2.072(8)	Ag1–C1^{1}	2.072(8)
Ag2–C2	2.054(8)	Ag2–C3	2.063(8)
Bond angle (°)			
N3^{2}–Fe1–N3	179.5(3)	N3^{2}–Fe1–N2	89.76(13)
N3–Fe1–N2	89.76(13)	N3–Fe1–N1	89.79(19)
N3^{2}–Fe1–N1^{2}	89.80(19)	N3–Fe1–N1^{2}	90.22(19)
N3^{2}–Fe1–N1	90.21(19)	N3^{2}–Fe1–N4^{3}	90.24(13)
N3–Fe1–N4^{3}	90.24(13)	N2–Fe1–N1^{2}	90.96(12)
N2–Fe1–N1	90.96(12)	N2–Fe1–N4^{3}	180.0
N1–Fe1–N1^{2}	178.1(2)	N4^{3}–Fe1–N1	89.04(12)
N4^{3}–Fe1–N1^{2}	89.04(12)	C1^{1}–Ag1–C1	180.00(6)
C2–Ag2–C3	180.0		

Symmetry transformations used to generate equivalent atoms: ^{1}1-X,1-Y,2-Z; ^{2}1-X,+Y,3/2-Z; ^{3}+X,-1+Y,+Z

Compound 1$^{298\ K}$			
Bond length (Å)			
Fe1–N1	2.206(6)	Fe1–N1^{2}	2.206(6)
Fe1–N2	2.110(8)	Fe1–N3	2.075(9)
Fe1–N3^{2}	2.075(9)	Fe1–N4^{3}	2.140(9)
Ag1–C1	1.966(12)	Ag1–C1^{1}	1.966(12)
Ag2–C2	2.045(13)	Ag2–C3	2.042(13)
Bond angle (°)			
N1–Fe1–N1^{2}	177.8(3)	N2–Fe1–N1^{2}	91.11(16)
N2–Fe1–N1	91.11(15)	N2–Fe1–N4^{3}	180.0
N3^{2}–Fe1–N1^{2}	90.0(3)	N3^{2}–Fe1–N1	90.0(3)
N3–Fe1–N1	90.0(3)	N3–Fe1–N1^{2}	90.0(3)
N3–Fe1–N2	89.0(2)	N3^{2}–Fe1–N2	89.0(2)
N3^{2}–Fe1–N3	178.0(4)	N3–Fe1–N4^{3}	91.0(2)
N3^{2}–Fe1–N4^{3}	91.0(2)	N4^{3}–Fe1–N1^{2}	88.89(15)
N4^{3}–Fe1–N1	88.89(16)	C1–Ag1–C1^{1}	180.0
C3–Ag2–C2	180.0		

Symmetry transformations used to generate equivalent atoms: ^{1}2-X,1-Y,2-Z; ^{2}2-X, +Y,3/2-Z;^{3}+X,-1+Y,+Z

Table S2. Average Fe1–N bond lengths (Å) for **1** at 120 and 298 K.

1	298 K	120 K
Fe1-N1	2.206(6)	2.022(4)
Fe1-N2	2.110(8)	1.977(7)
Fe1-N3	2.075(9)	1.953(5)
Fe1-N4	2.140(9)	1.980(7)
$Fe1\text{-}N_{average}$	2.132(7)	1.983(1)

Table S3. Mössbauer spectra parameters for **1** at 40 K.

T	δ	ΔE_Q	Relative area	
(K)	mm s^{-1}	mm s^{-1}	%	Fe type
40 K	1.08	2.10	19	Fe_{HS}^{II}
	0.39	0.16	81	Fe_{LS}^{II}

Table S4. The dielectric constant changes $\Delta\varepsilon'$ in the SCO compounds in the previous papers.

Year	Complex	Frequency	$\Delta\varepsilon' = \lvert \varepsilon'_{HS} - \varepsilon'_{LS} \rvert$	Ref
2003	$[Fe_{0.85}Zn_{0.15}(NH_2trz)_3](NO_3)_2$	10 kHz	0.008	1[2]
	$Fe(phen)_2(NCS)_2$		0.015	
	$Fe(bt)_2(NCS)_2$		0.15	
	$Fe_{0.8}Ni_{0.2}(btr)_2(NCS)_2 \cdot H_2O$		0.03	
2006	$[Fe(L)(CN)_2] \cdot H_2O$	100 kHz	0.18	2[3]
2017	$Fe(R\text{-}L^1)(bpz)_2$	1000 kHz	0.58	3[4]
	$Fe(S\text{-}L^1)(bpz)_2$	1000 kHz	0.46	
2018	$[(Tp)Fe^{III}(CN)_3]_2[Fe^{II}(azp)] \cdot 4H_2O$	1000 kHz	1.1	4[5]
2020	$[Fe^{II}(L)(bpy)]_n$	0.5 kHz	~9	5[6]
		1000 kHz	~0.9	
2022	$[Fe^{II}(dpa)][(pzTp)Fe^{III}(CN)_3]_2$	1000 kHz	2.3	6[7]
2022	$\{Fe(bpt)[Pt(CN)_4]\} \cdot 0.5anth$	100 kHz	~2.5	7[8]
This work	$\{Fe(DPPE)_2[Ag(CN)_2]_2\} \cdot 2EtOH$	0.5 kHz	1.2	
		1000 kHz	0.9	

Table S5. SHAPE analysis of Fe^{II} in compound **1** at 120 K and 298 K.

HP (D_{6h}): Hexagon; PPY (C_{5v}): Pentagonal pyramid; OC(O_h): Octahedron; TPR (D_{3h}): Trigonal prism; JPPY (C_{5v}): Johnson pentagonal pyramid J2.

Compond **1**					
	HP (*D6h*)	PPY (*C5v*)	OC （Oh）	TPR （C3h）	JPPY (*C5v*)
298 K	33.353	29.223	0.091	16.194	32.581
120 K	33.256	29.76	0.029	16.395	33.212

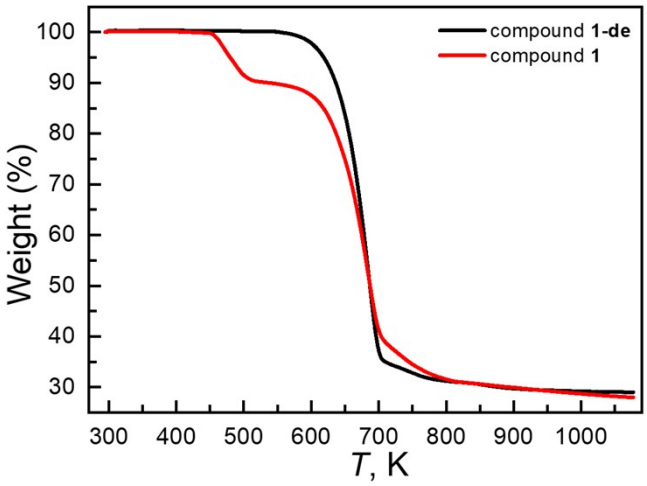

Figure S1. Thermo-gravimetric analysis curve for compound **1** and **1-de** in the nitrogen atmosphere with the sweeping rate of 10 K min^{-1}.

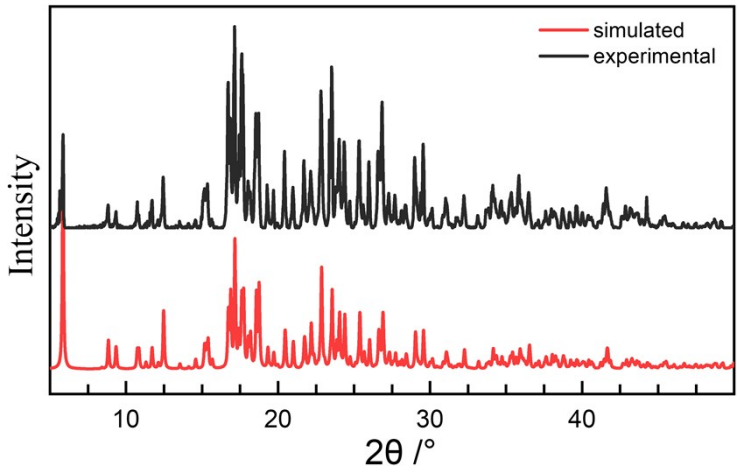

Figure S2. Powder X-ray diffraction data for compound **1** at room temperature.

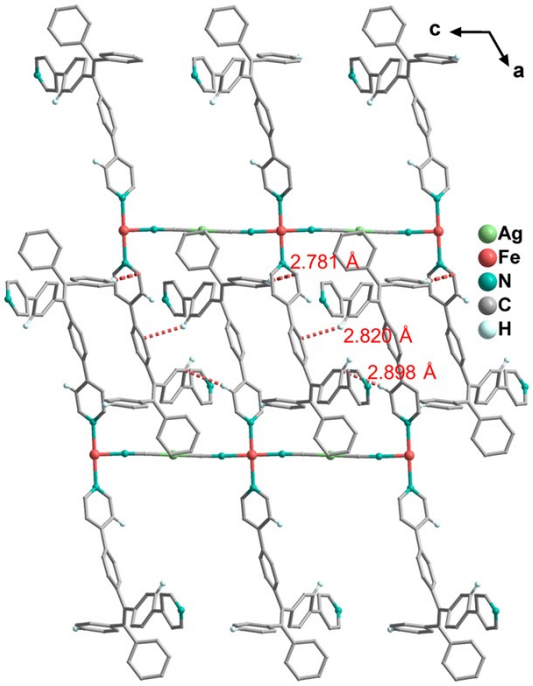

Figure S3. The interlayer short-contact interactions between DPPE ligands with the distances of 2.898 Å, 2.820 Å and 2.781 Å at 298 K and 2.828 Å, 2.750 Å and 2.613 Å at 120 K.

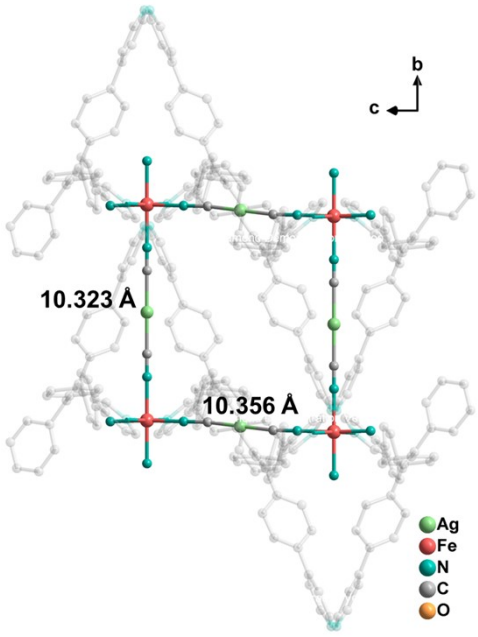

Figure S4. The Fe···Fe distances with the distances of 10.323, 10.356 Å at 120 K and 10.594, 10.591 Å at 298 K in **1**.

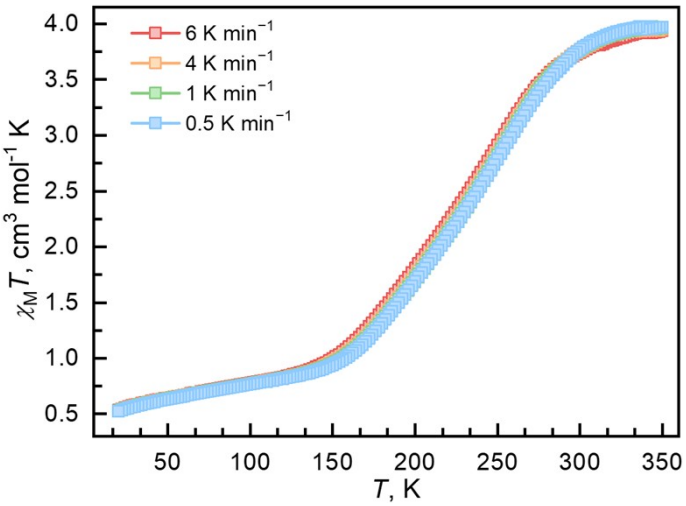

Figure S5. Scan rate study of temperature-dependent susceptibilities of compound **1** under the scan rates of 0.5, 1, 4, and 6 K min^{-1} over the temperature range of 20–350 K.

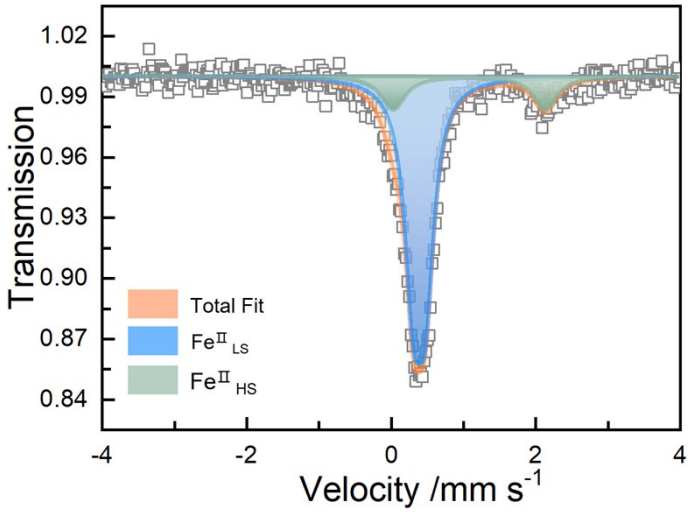

Figure S6. The Mössbauer spectra for **1** at 40 K.

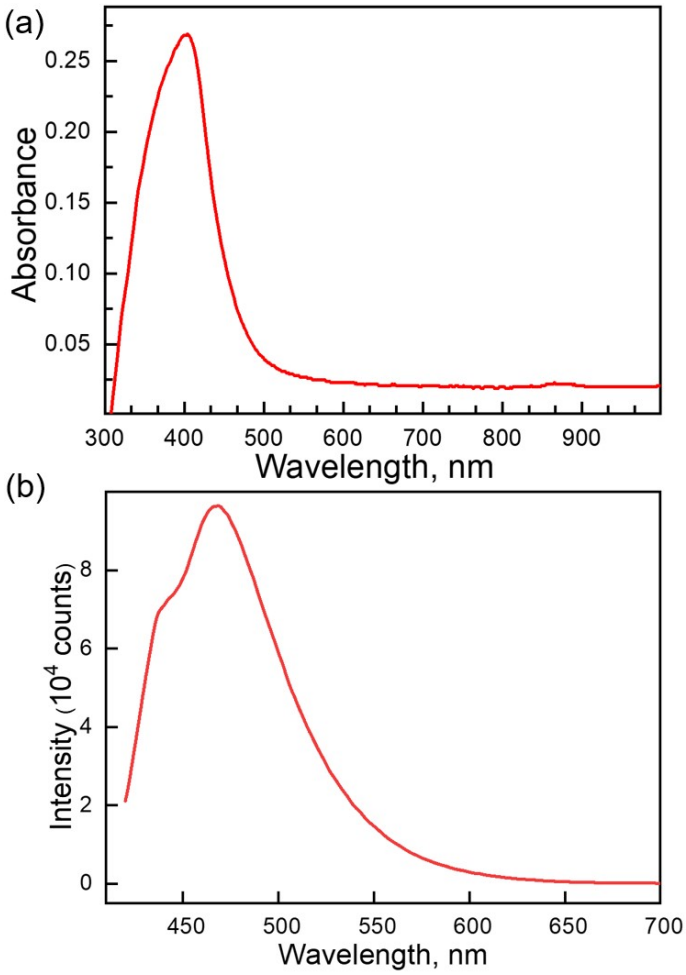

Figure S7. UV-vis spectrum (a) and fluorescence emission spectrum (b) of DPPE in solid at room temperature.

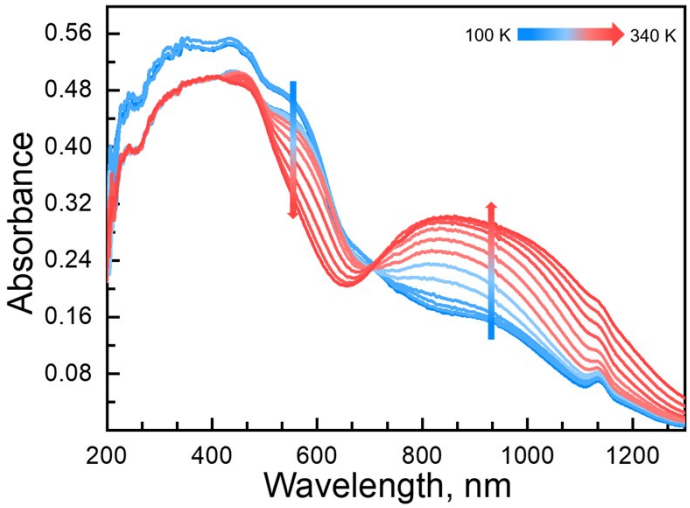

Figure S8. Temperature-dependent UV-vis spectra of **1** in a solid from 100 to 340 K in heating mode.

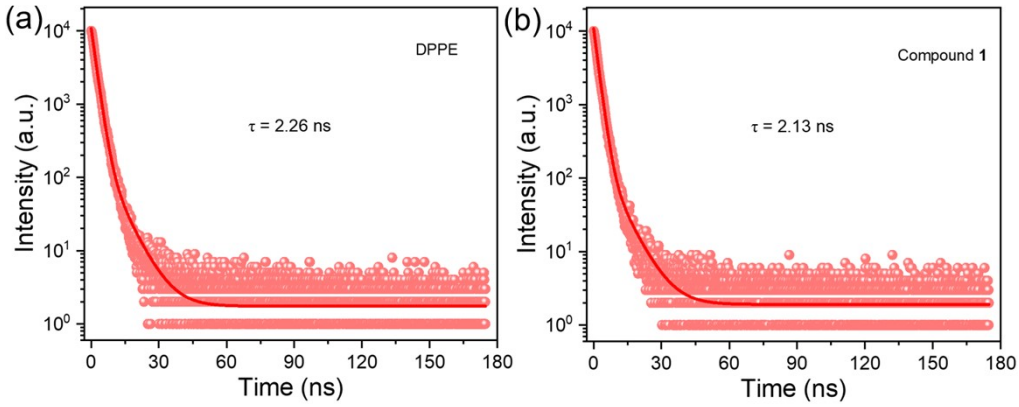

Figure S9. Luminescence decays of DPPE ligand and compound **1** in the solid at room temperature. The red line represented the fitting result.

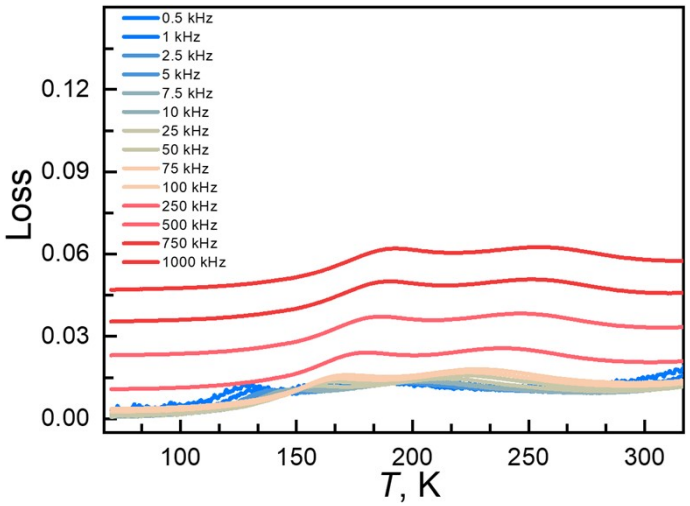

Figure S10. Temperature-dependent imaginary part of dielectric constants for **1**.

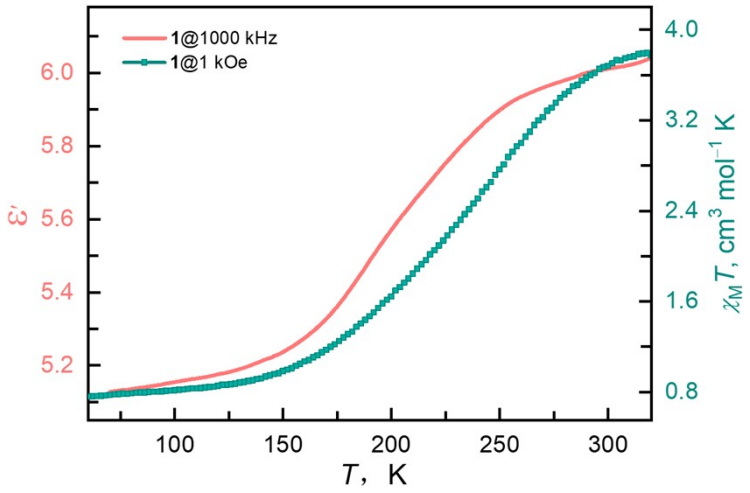

Figure S11. Temperature-dependent $\chi_M T$ products (cyan line) under the 1 kOe dc field and temperature-dependent dielectric constants (red line) at 1000 kHz for **1**.

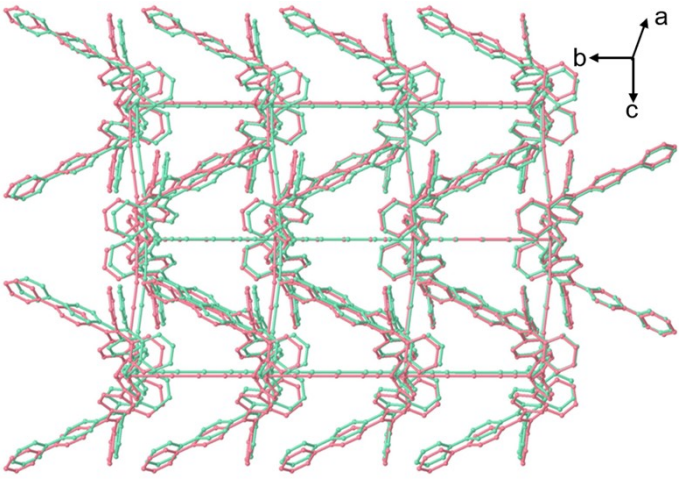

Figure S12. The overlapped diagram of molecular structures for **1** at 120 (green) and 298 K (red). Hydrogen atoms and solvent molecules were omitted for clarity.

References

[1] H. Ma, M. Yang, C. Zhang, Y. Ma, Y. Qin, Z. Lei, L. Chang, L. Lei, T. Wang and Y. Yang, *J. Mater. Chem. B*, 2017, **5**, 8525.

[2] A. Bousseksou, G. Molnár, P. Demont and J. Menegotto, *J. Mater. Chem.*, 2003, **13**, 2069−2071.

[3] S. Bonhommeau, T. Guillon, L. M. Lawson Daku, P. Demont, J. Sanchez Costa, J.-F. Létard, G. Molnár and A. Bousseksou, *Angew. Chem. Int. Ed.*, 2006, **45**, 1625−1629.

[4] J. Ru, F. Yu, P.-P. Shi, C.-Q. Jiao, C.-H. Li, R.-G. Xiong, T. Liu, M. Kurmoo and J.-L. Zuo, *Eur. J. Inorg. Chem.*, 2017, **2017**, 3144−3149.

[5] H. Zheng, Y.-S. Meng, G.-L. Zhou, C.-Y. Duan, O. Sato, S. Hayami, Y. Luo and T. Liu, *Angew. Chem. Int. Ed.*, 2018, **57**, 8468−8472.

[6] Y.-R. Qiu, L. Cui, P.-Y. Cai, F. Yu, M. Kurmoo, C. F. Leong, D. M. D'Alessandro and J.-L. Zuo, *Chem. Sci.*, 2020, **11**, 6229.

[7] W. Wen, Q. Liu, S.-H. Zhang, N.-T. Yao, H. Oshio, Y.-S. Meng and T. Liu, *Angew. Chem. Int. Ed.*, 2022, **61**, e202208886.

[8] N.-T. Yao, L. Zhao, H.-Y. Sun, C. Yi, Y.-H. Guan, Y.-M. Li, H. Oshio, Y.-S. Meng and T. Liu, *Angew. Chem. Int. Ed.*, 2022, **61**, e202208208.